



Original article

CoMFA, LeapFrog and blind docking studies on sulfonanilide derivatives acting as selective aromatase expression regulators

Carlos Gueto, Juan Torres, Ricardo Vivas-Reyes*

Grupo de Química Cuántica y Teórica, Universidad de Cartagena, Programa de Química, Facultad de Ciencias Exactas y Naturales, Campus De Zaragocilla, Cartagena, Colombia

ARTICLE INFO

Article history:

Received 12 September 2008

Received in revised form

2 February 2009

Accepted 9 February 2009

Available online 15 February 2009

Keywords:

SAERs

Sulfonanilide

3D-QSAR

CoMFA

Blind docking

eHiTS

LeapFrog

ABSTRACT

Aromatase, the enzyme responsible for estrogen biosynthesis, is an attractive target in the treatment of hormone-dependent breast cancer. In this manuscript, the structure-based drug design approach of sulfonanilide analogues as potential selective aromatase expression regulators (SAERs) is described. Receptor-independent CoMFA (Comparative Molecular Field Analysis) maps were employed for generating a pseudocavity for LeapFrog calculation. A robust model, using 45 and 10 molecules in the training and test sets, respectively, was developed producing statistically significant results with cross-validated and conventional correlation coefficients of 0.656 and 0.956, respectively. This model was used to predict the activity of newly proposed molecules as SAERs candidates being two magnitude orders more potent than the previously reported compounds. Also in the present study, the computational blind docking method using eHiTS is tested on molecules study group and COX-2 enzyme. Future perspectives of the method in the screening of SAERs candidates with no COX-2 inhibitory activity are discussed.

© 2009 Elsevier Masson SAS. All rights reserved.

1. Introduction

About one-third of breast cancers are estrogen receptor-positive (ER-positive or ER+), which are characterized by cells containing a significant number of estrogen receptors and requiring of estrogen for tumor growing. In post-menopausal patients this index rises to two-thirds [1]. For a long time, two hormonal approaches for treating ER+ breast cancer have been used: The first one consists of blocking the estrogen action mechanism by the selective estrogen receptor modulators (SERMs). All of the SERMs bind to the estrogen receptor and doing so, they reduce the available number for the endogenous estrogens [2]. The second way to deal with this pathology is with aromatase inhibitors (AIs). These ones work by inhibiting the action of the enzyme aromatase, which converts androgens into estrogens by a process called aromatization. As breast tissue is stimulated by estrogens, decreasing their production is a way of suppressing recurrence of the breast tumor tissue. Recent studies have shown that the third generation AIs are much more effective than Tamoxifen, the first antiestrogen used as hormonal therapy in ER+ breast cancer patients [3]. Nevertheless, these compounds inhibit the aromatase activity throughout the

body, causing side effects in areas such as bones and brain, where estrogens are required for their normal functioning [4]. As a consequence, to reduce the risk of the long-term side effects, a new pharmacological approach in the treatment of estrogen-dependent post-menopausal breast cancer is the use of tissue-specific inhibitors of aromatase. This concept is based on the tissue-specific regulation of aromatase expression.

A single gene, the CYP19, encodes the Cytochrome P450 human aromatase. Its structure shows some peculiarities: exons II–X encode the protein, while multiple alternative exons I encode unique 5'-untranslated regions of the aromatase mRNA transcripts [5]. Eight tissue-specific promoters control aromatase expression. A distinct set of transcription factors regulates each promoter [6–10]. In breast cancer tissues, aromatase expression switches from promoter I.4 to promoter I.3 and II [11]. Therefore, those drugs targeting the aromatase promoter I.3 and II-driven expression of this key enzyme become excellent chemotherapeutic agents for the ER+ breast cancers treatment. Besides, it has been shown that COX-1 and COX-2 inhibitors (Nonsteroidal anti-inflammatory drugs) can suppress the aromatase activity in SK-BR-3 breast cancer cells at transcriptional level [12], and consequently, the COX selective inhibitors could serve as the first generation of selective aromatase expression regulators (SAERs). Recently, the derivative analogue series of COX-2 inhibitors Nimesulide [13] and NS-398 [14] has been synthesized and tested in SK-BR-3 breast cancer cells [15–17],

* Corresponding author. Tel./fax: +57 5 6698180.

E-mail address: rvivasr@unicartagena.edu.co (R. Vivas-Reyes).

which suppress aromatase activity in breast cancer cells by suppressing its transcription [12]. Derivatives of NS-398 suppress aromatase activity at similar levels with the compound itself, whereas the *N*-methyl derivatives of NS-398 exhibit no COX-2 inhibition [15–17].

Quantitative structure–activity relationships (QSARs) allow researchers to establish *in silico* models in a reliable way to predict the activity of novel molecules before their synthesis. 3D-QSAR models have been successfully used to generate models of several chemotherapeutic agents. This computational technique has been used in a wide drug design of biological targets [18–20]. In order to study and infer a correlation between structure and biological activities, QSAR studies were carried out using comparative molecular field analysis (CoMFA) [21] for novel bioactive sulfonanilide analogues. This model, together with the contour maps derived, reveals the relevance of the steric and electrostatic fields. Structural variations in the molecular fields were studied in particular spatial regions according to the generated 3D-QSAR information using LeapFrog [22], a *de novo* ligand based design tool, and blind docking technique to give a deep insight in the novel SAERs study. Further, blind docking study on COX-2 protein was performed as a screening of SAERs candidates with no COX-2 inhibitory activity.

2. Computational details

2.1. Dataset for analysis

In vitro inhibitory activity data (IC₅₀ nM) of sulfonanilide analogues on SK-BR-3 breast cancer cell, reported by Su et al. [15–17] were taken for the study. Out of 66 aromatase gene expression inhibitors which were reported, 55 molecules (Tables 1–3) were selected for developing the model and 11 molecules whose IC₅₀ values were not quantitatively reported were not considered for the study. The dataset was randomly segregated into training and test sets (Tables 1–3) comprising 45 and 10, respectively.

2.2. Molecular conformation and alignment

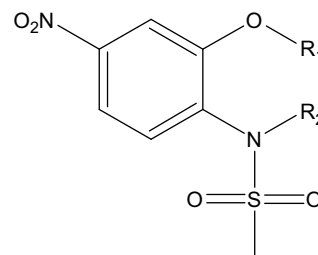
All molecular modeling studies were performed using the molecular modeling package SYBYL 7.0 [23]. The compounds were built from fragments in the SYBYL database. Tripos force field, conjugated gradient method, subsequently Gasteiger–Hückel [24] partial charges were calculated and the geometry of the molecules was optimized. The minimum gradient difference of 0.05 kcal/mol Å was set as a convergence criterion. After that, the lowest energy conformation found was led to an optimization by means of the HF/3-21g* [25] level using Gaussian 94 [26]. Since the specific molecular target of these compounds in breast cancer cells is unknown, the docking-based alignment method for developing a QSAR model could not be used. Instead, the most active molecule in the training set, compound **55** (Table 3), was chosen as the template and the whole set has to be superposed on the template conformation with the application of DATABASE ALIGNMENT method. The common substructure selected and aligned molecules are displayed in Fig. 1.

2.3. CoMFA analysis

The aligned molecules were placed in a 3D grid box such that the entire set was included in it. The steric (Lennard-Jones 6–12 potential) and electrostatic (Coulomb potential) field energies were calculated using sp³ carbon as probe atom and the standard TRIPOS force field was applied. The dielectric function was selected to be distance dependent. The energies were truncated to ±30 kcal mol^{−1}.

Table 1

Structures and biological activities of the training and test sets of molecules.



Mol	R ₁	R ₂	Actual ^a	CoMFA ^b	
				Pred	Δ
1	Cyclohexyl	H	−2.83	−2.88	0.05
2	Cyclohexyl	CH ₃	−2.67	−2.57	−0.10
3	Cyclopentyl	H	−2.94	−2.92	−0.02
4	Cyclopentyl	CH ₃	−2.64	−2.79	0.15
5	Methylcyclohexyl	H	−3.08	−3.03	−0.05
6 ^c	Methylcyclohexyl	CH ₃	−2.98	−3.10	0.12
7	1-Ethyl-propyl	H	−2.48	−2.51	0.03
8	1-Ethyl-propyl	CH ₃	−2.36	−2.33	−0.03
9	Propyl	H	−3.40	−3.36	−0.04
10 ^c	Propyl	CH ₃	−2.88	−3.31	0.43
11	Hexyl	H	−3.43	−3.47	0.04
12	Hexyl	CH ₃	−3.65	−3.51	−0.14
13	Nonyl	H	−2.96	−3.31	0.35
14	Nonyl	CH ₃	−3.60	−3.57	−0.03
15	Isopropyl	H	−3.77	−3.76	−0.01
16	Isopropyl	CH ₃	−3.45	−3.47	0.02
17 ^c	Benzyl	H	−3.33	−3.14	−0.19
18	Benzyl	CH ₃	−2.91	−2.96	0.04
19	4-Nitro benzyl	H	−2.60	−2.58	−0.02
20	4-Nitro benzyl	CH ₃	−2.69	−2.69	0.00
21	β-Naphthylmethyl	H	−3.34	−3.36	0.02
22	β-Naphthylmethyl	CH ₃	−3.43	−3.39	−0.04
23	2-Phenyl benzyl	H	−2.41	−2.39	−0.02
24	2-Phenyl benzyl	CH ₃	−2.52	−2.53	0.01
25 ^c	4-Methyl benzyl	H	−3.24	−3.41	0.17
26	4-Methyl benzyl	CH ₃	−3.37	−3.28	−0.09
27	4-Methoxy benzyl	H	−3.89	−3.40	−0.49
28	4-Methoxy benzyl	CH ₃	−2.67	−2.65	−0.02
29	4-Isopropyl benzyl	H	−3.87	−3.86	−0.01
30	4-Fluoro benzyl	H	−2.76	−2.69	−0.07
31 ^c	4-Fluoro benzyl	CH ₃	−3.25	−2.96	−0.29
32 ^c	4-Chloro benzyl	H	−2.46	−2.74	0.28
33	4-Chloro benzyl	CH ₃	−3.38	−2.99	−0.39
34	4-Bromo benzyl	H	−3.77	−3.26	−0.51
35	4-Bromo benzyl	CH ₃	−2.52	−2.62	0.10
36	4-Phenyl benzyl	H	−2.93	−2.92	−0.02
37	4-Phenyl benzyl	CH ₃	−2.81	−2.76	−0.05
38	Phenylethyl	H	−2.36	−2.44	0.08
39	Phenylethyl	CH ₃	−2.72	−2.70	−0.02
40 ^c	α-Naphthylmethyl	H	−3.76	−3.25	−0.51
41	α-Naphthylmethyl	CH ₃	−3.07	−3.10	0.03
42	Phenyl	H	−4.43	−4.41	−0.02
43	2,5-Dimethyl benzyl	H	−2.57	−2.59	0.02

^a Biological activity (nmol L^{−1}) expressed as −log IC₅₀ against human aromatase gene expression.

^b Calculated activity from CoMFA model.

^c Test set molecules.

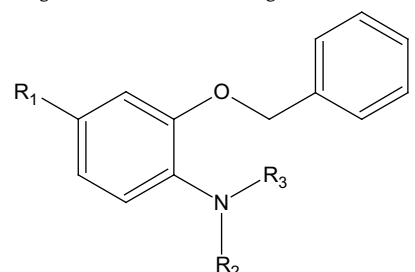
The CoMFA fields generated automatically were scaled by the CoMFA-STD method in SYBYL.

2.4. Partial least square (PLS) analysis

The CoMFA descriptors were used as independent variables and pIC₅₀ values as a dependent variable in PLS regression analysis in deducing the 3D-QSAR model. Normally, cross-validation is employed to check the predictivity of the derived model. The performance of models was calculated using the *leave-one-out* (LOO) cross-validation

Table 2

Structures and biological activities of the training and test sets of molecules.



Mol	R ₁	R ₂	R ₃	Actual ^a	CoMFA ^b	
					Pred	Δ
44 ^c	NO ₂	COCH ₃	H	−3.07	−3.12	0.05
45	NO ₂	4-Nitro-benzene sulfonyl	H	−3.34	−3.32	−0.02
46	NO ₂	4-Methyl-benzene sulfonyl	H	−4.24	−4.31	0.07
47	NH ₂	Methanesulfonyl	CH ₃	−3.04	−3.06	0.02

^a Biological activity (nmol L^{−1}) expressed as $-\log IC_{50}$ against human aromatase gene expression.^b Calculated activity from CoMFA model.^c Test set molecules.

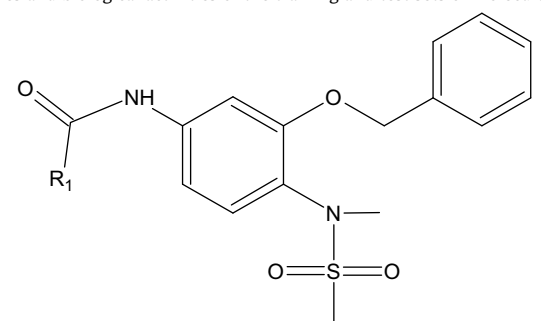
method. The optimum number of components used to derive the non-cross-validated model was defined as the number of components leading to the highest R² cross-validated and lowest standard error of prediction (SEP). To obtain the statistical confidence limit in analyses, PLS analysis using 100 bootstrap groups within the optimum number of components was performed.

2.5. Hypothetical cavity generation using LeapFrog

LeapFrog is a second-generation *de novo* tool to design a series of potential active ligand molecules even when the receptor structure is unknown [27]. This drug discovery program can start from either of two kinds of information: a cavity from the receptor structure or, in our case, a pharmacophoric model, which is expressed as CoMFA

Table 3

Structures and biological activities of the training and test sets of molecules.



Mol	R ₁	Actual ^a	CoMFA ^b	
			Pred	Δ
48 ^c	Methyl	−4.22	−3.75	−0.47
49	Phenyl	−3.25	−3.21	−0.04
50	Cyclohexanyl	−2.40	−2.39	−0.01
51	3,4-Dichloro phenyl	−2.84	−2.85	0.01
52	4-Chloro-3-nitro phenyl	−2.84	−2.79	−0.05
53 ^c	4-Cyano phenyl	−2.64	−2.66	0.02
54	2-Naphthalene	−3.03	−3.06	0.03
55	4-Biphenyl	−2.08	−2.08	0.00

^a Biological activity (nmol L^{−1}) expressed as $-\log IC_{50}$ against human aromatase gene expression.^b Calculated activity from CoMFA model.^c Test set molecules.

model. As the target of the sulfonamide analogues is not determined, the latter approach was implemented for proposing new molecules as potential inhibitors of aromatase expression. Binding energy calculations in LeapFrog are performed by three major components viz., direct steric, electrostatic, and implicit hydrogen bonding enthalpies of ligand–cavity binding using the Tripos force field. In LeapFrog, ligand atom coordinates are binned to increase speed and the binding energy of each ligand atom is calculated as though the atom were actually located in the center of a cube containing that atom. Next, a simple linear expression yields the energy of interaction between the site and that particular ligand atom. Summing overall ligand atoms yields the overall site–ligand interaction energy. The program also allows use of optional cavity desolvation energy, an optional incremental hydrogen bonding energy, and optional ligand desolvation energy, estimated from a very simple model.

LeapFrog makes use of the CoMFA contours for the generation of its cavity. There are two distinct ways to perform this process. One is by direct point-by-point mapping of the properties of a CoMFA grid to an intermediate cavity grid of the same coarse resolution, and the other is by interpolation of the intermediate cavity grid values to the closely spaced grid values actually used by LF. The cavity thus obtained was used to generate the site points. The charge of a site point atom is positive, negative, or lipophilic. Its value is compared with 1.0. If the atom charge is smaller in magnitude than 1.0 the site point is lipophilic; if greater than +1.0, the site point seeks a negative atom; and if less than −1.0, the site point seeks a positive atom in the approaching fragment.

2.6. eHiTS blind docking

Molecular docking has been proven to be an important tool of computer-aided drug design. Most computational docking applications study the binding modes of ligands by utilizing prior knowledge of binding sites. Therefore the docking area is usually limited to a specific protein region. Recently, the concept of *blind docking* has been explored to scan entire protein for potential drug binding sites [28]. Herein the concept of blind docking was implemented in order to reproduce the experimental observation that only the NH-bearing sulfonamide derived molecules may act on the COX-2 binding pocket [29,30]. Furthermore it was explored what type of NH-bearing sulfonamide derived molecules binds the active site of the enzyme when docking calculation was performed. For this aim, eHiTS 6.2 (electronic High Throughput Screening), a new, fast, exhaustive flexible ligand docking with a systematic algorithm program was used [31,32]. In eHiTS, the search algorithm is based on exhaustive graph matching that rapidly enumerates all possible mappings of interacting atoms between receptor and ligand. eHiTS divides a ligand into rigid fragments or nodes that are docked separately in receptor and stores rigid fragment poses in DockTable, an SQL database that increases the speed of dockings by dynamically updating and retrieving molecular fragments during the docking process. The scoring function contains treatment of weak hydrogen bonds, aromatic pi-stacking and penalties for conflicting interactions. For the present work, the coordinates of cyclooxygenase-2 enzyme crystal structure (1CX2) were retrieved from the Brookhaven Protein Database [33]. The SC-558 was deleted from the file and a single mol2 file was used to take the Cartesian coordinates of sulfonamide analogues compounds.

3. Results and discussion

3.1. Blind docking

The objective of this stage was to corroborate computationally that introduction of a methyl group at the N atom of sulfonamide

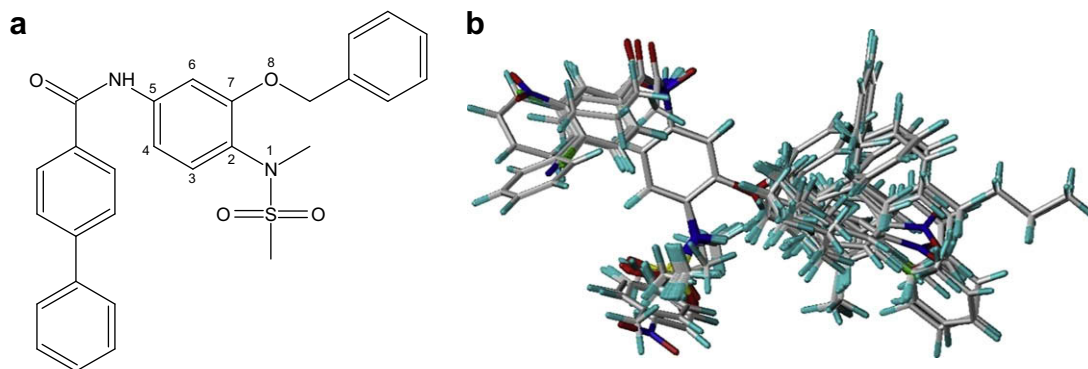


Fig. 1. (a) Structure of compound **55** and its atoms used for superposition (b) alignment of training and set molecules.

group to the sulfonanilide analogues resulted in no COX-2 inhibitory activity. As shown in Fig. 2 none of the *N*-methylated molecules bind the active site. This result is in line with the finding made by Su et al. [15–17] who determined that modulation of aromatase expression by NS-398 analogues does not necessarily require the inhibition of COX-2 enzyme activity [29,30]. Interestingly, some of the NH-bearing sulfonanilide derived molecules do not dock the active site either. This was observed in molecules with substitution of a bulky group at 1-, 2-, 4-positions of sulfonanilide analogues as can be seen in the case of compounds **1**, **3**, **5**, **18**, **23**, **25**, **36**, **38**, **43**, **46** and **55**. This arises the possibility of using blind docking for SAERs virtual screening to avoid side effects associated with COX-2 inhibitors such as the increased risk of myocardial infarction and stroke [34]. On the other hand, in several COX-2 ligand complexes it was observed H-bonds between the residues Ser530, Tyr355 and the oxygen atoms of the sulfonyl and nitro moieties of the ligand, respectively (Fig. 3). Similar interactions are also found in the diclofenac–COX-2 crystalline complex [35].

3.2. CoMFA analysis

CoMFA technique was used to derive a 3D-QSAR model on novel series of sulfonanilide analogues acting as SAERs. The biological activity negative logarithm was used as a dependent variable. CoMFA model was obtained with 45 and 10 molecules in the training and test sets respectively. Summary for the PLS analysis is

shown in Table 4. The actual, predicted and residuals of all set molecules are shown in Tables 1–3. The plot of actual versus predicted pIC_{50} of training and test set molecules is shown in Fig. 4. Fortunately, there is no outlier in the CoMFA model due to the generally, extrapolations of up to one order of magnitude (± 1 log unit) are acceptable. The largest residual is that compound **34** (-0.51), which still falls within 1 log unit.

In CoMFA method, results are presented as contour maps that correlate the change in biological activity with the molecular field values. The steric contour maps are represented in green and yellow colors while the electrostatic contours are depicted in red and blue colors. The green contours are indicative of favorable regions for sterically bulkier groups and the yellow contours are indicative of regions that are sterically less favorable. Similarly, the electrostatic red plots show the regions where the presence of a negative charge is expected to favor the activity whereas the blue contours are indicative of regions where introducing or keeping positive charges is expected to improve the observed activity. The contour maps are limited to the regions where various substituents have been modified. These variations are mainly at the oxygen tail group where a variety of substituents have been tested. The electrostatic and steric contours for most active molecule (compound **55**) are displayed in Fig. 5a and b, respectively (For interpretation of the references to colour in this figure legend, the reader is referred to the web version of this article.)

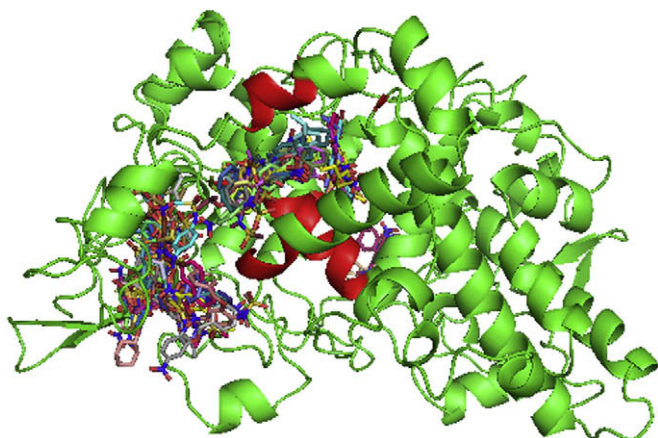


Fig. 2. Cartoon representation of the blind docking of the NS-398 analogues with the COX-2. The active site residues are shown in red (For interpretation of the references to colour in this figure legend, the reader is referred to the web version of this article.)

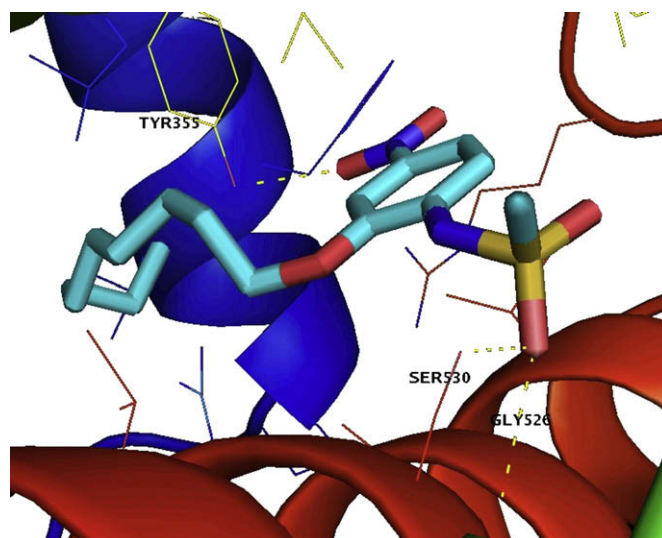
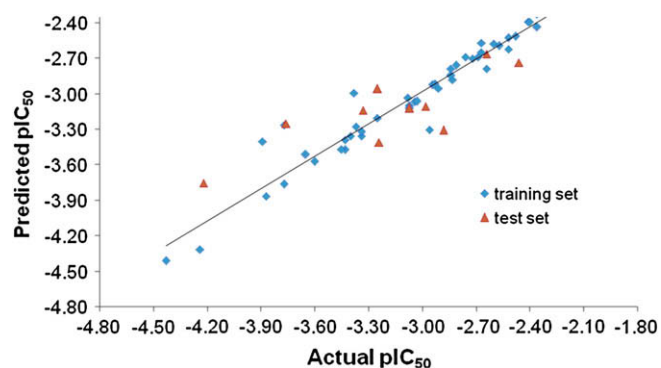
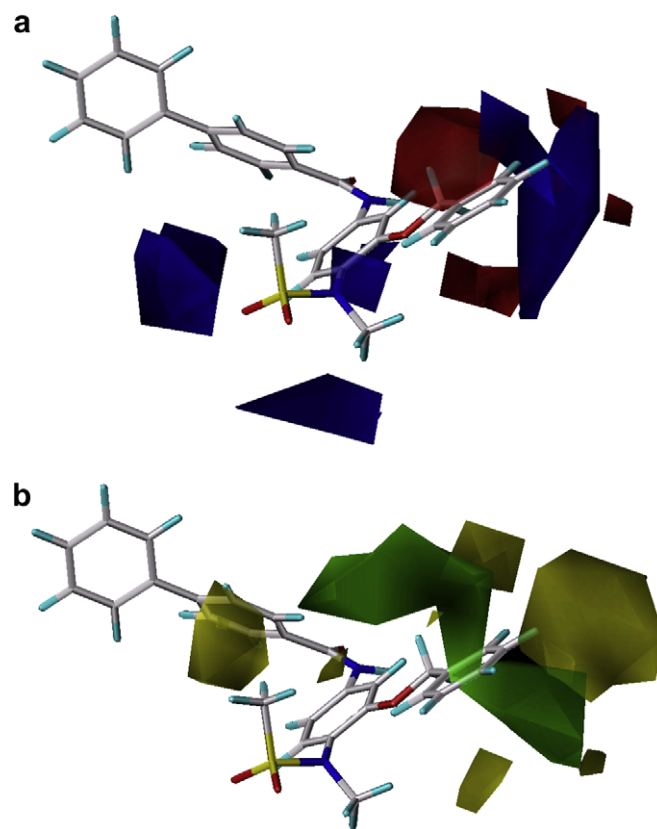


Fig. 3. Docked molecule **13** inside the COX-2 protein.

Table 4
Summary of CoMFA results.

R ² cross-validated (q ²)	0.656
Standard error of prediction	0.391
Number of components	7
Non-cross-validated R ²	0.956
Standard error of estimate	0.073
F value	259.349
R _{bs} ² from 100 bootstrapping runs	0.989
Standard deviation	0.045
Probability of R ² = 0	0.000
Contributions	
Steric maps	60.4%
Electrostatic maps	39.6%

The CoMFA electrostatic map shows two red contours surrounding the phenyl ring while a prominent blue polyhedron is around of 2', 3' and 4' positions of phenyl ring (Fig. 5a). Compounds with groups in the 4-position with moderate electron-withdrawing capacity have a good inhibitory activity but just considering the *N*-methylated sulfonanilide ones, which do not act on COX-2 protein and usually are better SAERs; in the case of compounds with halogens, compounds **30–35**, the biological activity increases as atom-size rises and the electron-withdrawing capacity decreases. Spatial distribution of electrostatic contours is the reason for changes in inhibitory activity: The halogens are near to red polyhedrons but closer to the blue one and that is why compounds with –F and –Cl at 4-position of benzyl group, compounds **31** and **33**, respectively, have less biological activity than compound **35** which bears a –Br atom. Conversely, compounds with electron-releasing groups, compounds **25**, **26** and **29**, are in direct contact with a blue polyhedron which would increase the inhibitory activity but the two red contours antagonistically affect its ability like SAERs. Like a midpoint among previous molecules groups, compounds with moderate electron-withdrawing groups at 4-position of phenyl ring, such as compounds **20** and **28**, present their substituents in regions when they become favored for the entire electrostatic polyhedrons; compound **28**, with a methoxy group at 4-position of phenyl ring, has a oxygen atom in zones where the two red electrostatic contours are associated with electronegative substituents and enhanced activity whereas the methyl moiety is in direct contact with the big blue polyhedron, areas where the electro-positive properties of molecules indicate low electron density and an increase in its ability like SAER. On the other hand, the CoMFA steric map (Fig. 5b) encompasses sterically favorable contours (80% contribution) corresponding to regions in space where steric bulk envisages the enhanced activity and the big green polyhedron bordering the phenyl ring of compound **81** reveals that an increase in activity is anticipated due to the increased steric bulk. This also

**Fig. 4.** Graph of actual versus calculated activities from CoMFA model.**Fig. 5.** CoMFA STDEV \times COEFF (a) electrostatic and (b) steric contour maps. The most active molecule **55** is displayed in the background.

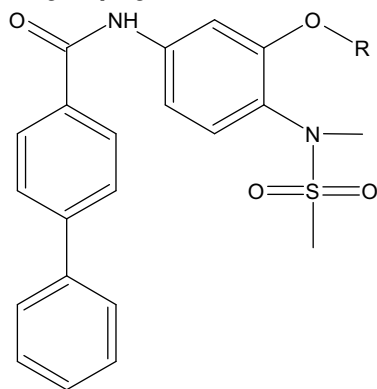
accounts for molecules with substitution of a bulky group at 2-position of sulfonanilide analogues as can be seen in the case of compounds **1–4**, **9**, **18**, **23**, **24**, **36**, **37** and **43**. Further, a sterically unfavorable region (20% contribution), yellow polyhedron, bordering the groups around 4-position of phenyl ring reveals that small moieties, such as methyl (compounds **25** and **26**), nitro (compounds **19** and **20**) and halogens (compounds **30–35**), will enhance the ability to suppress aromatase activity. The relative flexibility of the moieties at 2-position of sulfonanilide derived compounds appears to affect the biological activity too: Nimesulide, compound **42**, which bears a phenyl group has a poor ability like SAER. Though, extending one and two carbon at the 2-position of Nimesulide gets compounds **17** and **38**, respectively, which turns out in a significant rise in the suppression of aromatase compared with Nimesulide. Apparently, the structural flexibility of the aliphatic chain moieties seems to allow it to maneuver the phenyl ring moiety into the ideal space in the target pocket at the same time that forms new attractive hydrophobic interactions. Compounds with flexible aliphatic substituents at 2-position of sulfonanilide analogues such as compounds **5–8** and **10**, bear a good inhibitory activity too. In addition, electrostatic and steric unfavorable contours (20% contribution) bordering the methyl tail of the methanesulfonyl moiety suggest that small and electropositive groups enhance the activity. Therefore, bulkier substituents like 4-methyl-benzene sulfonyl in compound **46** are not favorable in that region. The present results of 3D-QSAR studies are in agreement with biological aromatase breast cancer cell test inhibitory activity as reported by Su et al. and act as the guidance source for the design of new molecules from the existing ones, with improved biological activity.

3.3. LeapFrog analysis calculations

The results of PLS analysis described above and the region file of the contour were used for cavity generation calculations for our study. Compound **55**, the most biologically active compound of the training set, was submitted for LeapFrog optimization. Thus, the hypothetical cavity using CoMFA maps was used along with the NEW move in LeapFrog to generate the novel ligands, which were then built using other moves such as JOIN, FUSE, COMPLEMENT, BRIDGE, and OPTIMIZE. The new ligands were checked for alternative orientations using FLY and were completely minimized using TWIST move to evaluate the binding energy for the minimum energy conformation of the ligand. The process was repeated to generate the different classes of ligands, which are described above. The ligands, which showed binding, better than the reference structure were taken up for quantum mechanics optimization and alignment to compound **55** according to the methodology described above. The relative LeapFrog binding energy and pIC_{50} CoMFA prediction of the top ten molecules design are shown in Table 5 and Fig. 6 represents a view of the site points generated by LeapFrog and the molecule with the best binding energy– pIC_{50} CoMFA prediction relationship, compound **61**, is shown in the background. The blue spheres represent hydrogen bonding acceptor site points while the red spheres represent donor site points. The blind docking results indicate that none of the design molecules exhibited in Table 5 bind to the COX-2 active site pocket.

The CoMFA electrostatic contour plot for compound **61** is shown in Fig. 7a (For interpretation of the references to colour in this figure legend, the reader is referred to the web version of this article.) The blue contours (80% contribution) are found in the vicinities of biphenyl ring and methanesulfonyl moieties, which define areas where the electropositive properties will result in enhanced activity. Red contours (20% contribution) observed close to the oxygen linker and nitro moieties suggest that increased activity is anticipated by

Table 5
Molecular design through LeapFrog.



Mol	R	B.E. ^a	CoMFA ^b
55	Benzyl	−783.09	−2.08
56	4-Methoxy benzyl	−2056.67	−1.38
57	4-Nitro benzyl	−1965.92	0.81
58	4-Phenyl benzyl	−2093.81	−1.13
59	2-Phenyl benzyl	−1822.48	−1.63
60	2,5-Dimethyl benzyl	−2039.37	−1.58
61	2-Phenyl-4-nitro benzyl	−2062.74	0.83
62	2-Phenyl-4-methoxy benzyl	−1965.77	−1.27
63	2-Phenyl-5-methyl benzyl	−2098.00	−1.84
64	2-Phenyl-4-methoxy-5-methyl benzyl	−1665.06	−0.89
65	2-Phenyl-4-nitro-5-methyl benzyl	−1454.05	−0.24

^a Binding energy (kcal mol^{-1}).

^b Predicted pIC_{50} from CoMFA model.

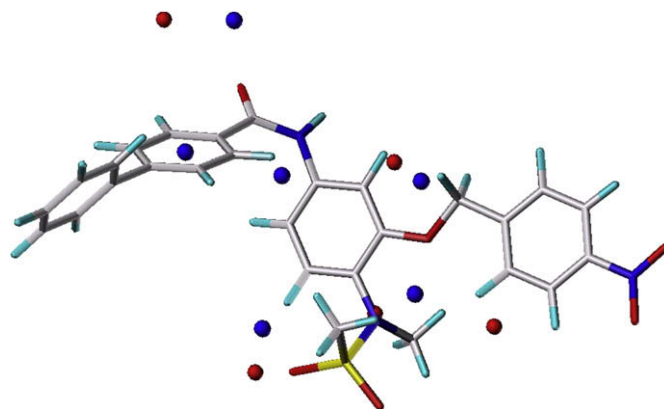


Fig. 6. The site points generated by LeapFrog along with molecule **61**.

electronegative property of this atom. The CoMFA contour maps (Fig. 7b) encompass sterically unfavorable contours (20% contribution) close to bordering the methanesulfonyl and nitro moieties whereas sterically favorable polyhedrons are in the vicinity of the phenyl ring yielding, in both cases, an enhanced biological activity.

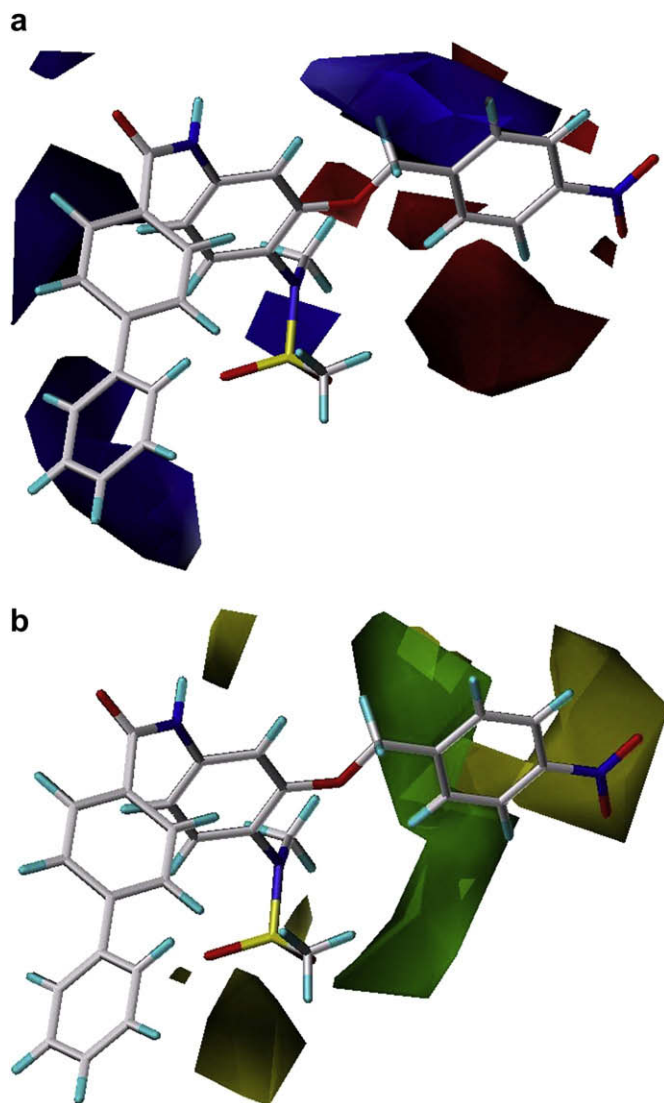


Fig. 7. CoMFA STDEV \times COEFF contour maps: (a) steric and (b) electrostatic fields around the optimized compound **61**.

4. Conclusion

A receptor-independent 3D-QSAR analysis, CoMFA was used to build statistically significant model with good correlative power for aromatase expression and inhibitory activity of the sulfonanilide derivates. The robustness of the derived model was verified by bootstrapping method. LeapFrog was an attempt to design molecules based on the concept of hypothetical cavity generation using CoMFA contours which yield new compounds with greater potency than the original ones. Blind docking technique using eHiTS was successful to reproducing the fact that, introduction of a methyl group at the N atom of sulfonamide group to the sulfonanilide analogues resulted in no COX-2 inhibitory activity. Herein our CoMFA model and the other techniques can be used strategically in the design of novel, potent SAERs as anticancer therapeutic agents.

Acknowledgments

Financial support to this work from National Institute of Science and Technology (Colciencias) of the Republic of Colombia (Bogota – Colombia) and the Universidad de Cartagena (Cartagena – Colombia) is highly appreciated.

References

- [1] L.J. DeGroot, J.L. Jameson, H.G. Burger, et al., in: N.L. Weigel, B.G. Rowan (Eds.), *Endocrinology*, WB Saunders, Philadelphia, 2001, p. 2053.
- [2] P.L. Carmichael, *Cancer Invest.* 16 (1998) 604–611.
- [3] M. Baum, A.U. Budzar, J. Cuzick, J. Forbes, J.H. Houghton, J.G. Klijn, T. Sahmoud, *Lancet* 359 (2002) 2131–2139.
- [4] H.M. Heshmati, S. Khosla, S.P. Robins, W.M. O'Fallon, L.J. Melton, B.L. Riggs, *J. Bone Miner. Res.* 17 (2002) 172–178.
- [5] G. Galmiche, S. Corvaisier, M. Kottler, *Ann. N.Y. Acad. Sci.* 1070 (2006) 286–292.
- [6] E.R. Simpson, *Semin. Reprod. Med.* 22 (2004) 11–23.
- [7] S. Chen, *Front. Biosci.* 3 (1998) 922–933.
- [8] C. Zhou, D. Zhou, J. Esteban, J. Murai, P.K. Siiteri, S. Wilczynski, S. Chen, *J. Steroid Biochem. Mol. Biol.* 59 (1996) 163–171.
- [9] Y. Zhao, C.R. Mendelson, E.R. Simpson, *Mol. Endocrinol.* 9 (1995) 340–349.
- [10] D. Zhou, P. Clarke, J. Wang, S.J. Chen, *J. Biol. Chem.* 271 (1996) 15191–15202.
- [11] D. Zhou, C. Zhou, S.J. Chen, *J. Steroid Biochem. Mol. Biol.* 61 (1997) 273–280.
- [12] E.S. Díaz-Cruz, C.L. Shapiro, R.W. Brueggemeier, *J. Clin. Endocrinol. Metab.* 90 (2005) 2563–2570.
- [13] B. Basel (Ed.), *Nimesulide – Actions and Uses*, SpringerLink, Sheffield, 2006.
- [14] J.P. Famaey, *Inflamm. Res.* 46 (1997) 437–446.
- [15] B. Su, E.S. Díaz-Cruz, S. Landini, R.W. Brueggemeier, *J. Med. Chem.* 49 (2006) 1413–1419.
- [16] B. Su, S. Landini, D. Davis, R.W. Brueggemeier, *J. Med. Chem.* 50 (2007) 1635–1644.
- [17] B. Su, R. Tian, M.V. Darby, R.W. Brueggemeier, *J. Med. Chem.* 51 (2008) 1126–1135.
- [18] C.N. Pramod, M.E. Sobhia, *J. Mol. Graphics Modell.* 26 (2007) 117–123.
- [19] C. Gueto, J.L. Ruiz, J.E. Torres, J. Méndez, R. Vivas-Reyes, *Bioorg. Med. Chem.* 16 (2008) 2439–2447.
- [20] J.H. Lee, N.S. Kang, S. Yoo, *Bioorg. Med. Chem. Lett.* 18 (2008) 2479–2490.
- [21] P.R. Jayatilake, A.C. Nair, R. Zauhar, W.J. Welsh, *J. Med. Chem.* 43 (2000) 4446–4451.
- [22] T.M. Mahindra, T.K. Rajesh, M.K. Vithal, N. Nouri, *J. Bioorg. Med. Chem.* 12 (2004) 2317–2333.
- [23] SYBYL, *Molecular Modeling System*, version 7.0, Tripos Inc., St. Louis, MO, 63144–2913.
- [24] J. Gasteiger, M. Marsili, *Tetrahedron* 36 (1980) 3219–3228.
- [25] K. Dobbs, W. Hehre, *J. Comput. Chem.* 8 (1987) 880–893.
- [26] *Gaussian 94*, Revision B.02, Gaussian, Inc., Pittsburgh, PA, 1995.
- [27] SYBYL, *Ligand-Based Design Manual*, version 7.0, Tripos Inc., St. Louis, MO.
- [28] C. Hetényi, D. van der Spoel, *Protein Sci.* 11 (2002) 1729–1737.
- [29] F. Julemont, X. de Leval, C. Michaux, J. Damas, C. Charlier, F. Dyrant, B. Pirotte, J.M. Dogné, *J. Med. Chem.* 45 (2002) 5182–5185.
- [30] G. Cignarella, P. Vianello, F. Berti, G. Rossoni, *Eur. J. Med. Chem.* 31 (1996) 359–364.
- [31] Z. Zsoldos, D. Reid, A. Simon, S.B. Sadjad, A.P. Johnson, *J. Mol. Graphics Modell.* 26 (2007) 198–212.
- [32] Z. Zsoldos, D. Reid, A. Simon, S.B. Sadjad, A.P. Johnson, *Curr. Protein Pept. Sci.* 7 (2006) 421–435.
- [33] R.G. Kurumbail, A.M. Stevens, J.K. Gierse, J.J. McDonald, R.A. Stegeman, J.Y. Pak, D. Gildehaus, J.M. Miyashiro, T.D. Penning, K. Seibert, P.C. Isakson, W.C. Stallings, *Nature (London)* 384 (1996) 644–648.
- [34] A.T. Chan, C.S. Fuchs, *Nat. Clin. Pract. Oncol.* 2 (2005) 434–435.
- [35] S.W. Rowlinson, J.R. Kiefer, J.J. Prusakiewicz, J.L. Pawlitz, K.R. Kozak, A.S. Kalgutkar, W.C. Stallings, R.G. Kurumbail, L.J. Marnett, *J. Biol. Chem.* 278 (2003) 45763–45769.